







Improving RF-Based Partial Discharge Localization via Machine Learning Ensemble Method

Ephraim Tersoo Iorkyase , Christos Tachtatzis , Ian A. Glover , Pavlos Lazaridis , David Upton ,
Bakhtiar Saeed , and Robert C. Atkinson

Abstract—Partial discharge (PD) is regarded as a precursor to plant failure and therefore, an effective indication of plant condition. Locating the source of PD before failure is key to efficient maintenance and improving reliability of power systems. This paper presents a low cost, autonomous partial discharge radiolocation mechanism to improve PD localization precision. The proposed radio frequency-based technique uses the wavelet packet transform (WPT) and machine learning ensemble methods to locate PDs. More specifically, the received signals are decomposed by the WPT and analyzed in order to identify localized PD signal patterns in the presence of noise. The regression tree algorithm, bootstrap aggregating method, and regression random forest are used to develop PD localization models based on the WPT-based PD features. The proposed PD localization scheme has been found to successfully locate PD with negligible error. Additionally, the principle of the PD location scheme has been validated using a separate test dataset. Numerical results demonstrate that the WPT-random forest PD localization scheme produced superior performance as a result of its robustness against noise.

Index Terms—Partial discharge, localization, wavelet packet transform, bootstrap aggregating, random forest, regression tree.

I. INTRODUCTION

THE presence of partial discharge in electrical assets is indicative of some defect in the insulation system of the device. These discharges can harm the insulation and might lead to total breakdown of the asset over time with social and economic consequences. The uninterrupted monitoring of these assets is therefore paramount in the operation of the electric power system. One of the leading candidates for effective condition monitoring of electrical assets is partial discharge [1], [2]. PDs are ionization processes that occur in void filled gases or liquids inside insulation, in dielectric surfaces, and in the proximity of

sharp metallic objects [3]–[5]. PDs emit part of the energy they produce as electromagnetic waves [6] and this has motivated the use of radio sensors for detection and localization of the discharge sources. Early detection of PD reduces the risks of harm to insulation and can prevent sudden breakdown. Once the occurrence of PD has been established, it is a matter of urgency to locate the discharge source as quickly and accurately as possible to enable corrective maintenance operation when the maintenance activity is most cost effective and before the equipment loses performance or suffers catastrophic failure.

RF-based PD location has been widely studied [7]–[11]. Given a model of radio signal propagation in a particular environment, the TDoA, AoA and/or RSS [5], [12]–[15] algorithm can be used to estimate the distance from a source to a receiver and thereby trilaterate the location of the PD. UHF antenna arrays [8] have also been used to locate impulsive PDs in a substation. In cables, time-domain reflectometry (TDR) [16] which is based on the time difference of arrival is used to locate the source of PD along a cable. The time-difference-of-arrival (TDoA) of the received signals is established by cross-correlation and the location of PD is found by multi-lateration [17]. Unfortunately, this technique is uneconomical and complex requiring accurate synchronization, and Line-of-Sight (LOS) propagation for accurate location estimation. It also requires a detailed RF propagation model for every environment in which this system is deployed and this is not trivial to obtain. The environment in which PD is expected is characterized by interference, multipath propagation and presence of metallic obstacles leading to a complex spatial radio environment, which is difficult to describe by ready-made models.

In previous work, we have adopted a pattern matching technique which uses features of the received radio signals to infer PD location [14]. The pattern matching technique can be regarded as a low cost technique compared to those based on time estimation [18]. It turns the frequency-selective multipath phenomenon to surprisingly good use: by combining the multipath pattern with other PD pulse characteristics, it creates unique RF signatures representing different locations.

In this study, we propose to deploy a spatial array of low cost off-the-shelf commercial radio sensors in form of wireless sensor network in an electricity substation. The proposed solution allows a PD monitoring system to be permanently deployed and thus monitor the substation uninterrupted in real-time and at low cost. In this approach, the network autonomously creates a spatial map of the RF characteristics of the radio signals and

Manuscript received June 29, 2018; revised December 21, 2018 and February 11, 2019; accepted March 17, 2019. Date of publication March 25, 2019; date of current version July 23, 2019. This work was supported in part by the Engineering and Physical Sciences Research Council under Grant EP/J015873/1 and in part by the Tertiary Education Trust Fund (TETFund) Nigeria. Paper no. TPWRD-00753-2018. (Corresponding author: Ephraim Tersoo Iorkyase.)

E. T. Iorkyase, C. Tachtatzis, and R. C. Atkinson are with the Department of Electronic and Electrical Engineering, University of Strathclyde, G1 1XW Glasgow, U.K. (e-mail: ephraim.iorkyase@strath.ac.uk; christos.tachtatzis@strath.ac.uk; robert.atkinson@strath.ac.uk).

I. A. Glover, P. Lazaridis, D. Upton, and B. Saeed are with the Department of Engineering and Technology, University of Huddersfield, HD1 3DH Huddersfield, U.K. (e-mail: I.A.Glover@hud.ac.uk; p.lazaridis@hud.ac.uk; D.W.Upton@hud.ac.uk; B.Saeed@hud.ac.uk).

Color versions of one or more of the figures in this paper are available online at <http://ieeexplore.ieee.org>.

Digital Object Identifier 10.1109/TPWRD.2019.2907154

uses sophisticated machine learning techniques to estimate the location of PD sources. In previous work we have used machine learning algorithms to build a bespoke propagation model for the radio environment from the perspective of each node [13]. Based on the relative received signal strength of a PD pulse at each node, a multilateration approach can be deployed to infer PD location. In this work, we go further by investigating the temporal signatures of the received pulses to determine if they are able to provide a more accurate estimation of location than raw energies alone.

One approach, we have considered, in engineering PD features for source localization is direct extraction from measured time domain PD signals. These features infer the location where PD originate and are referred to as location dependent parameters. Features extracted from time domain signals for PD location assume a single PD type scenario. However, localization of PD using such features may not be sufficient in real electricity substations where different types of PD occur. Therefore, we adopt a modified version of this approach by examining the time-domain signatures from each pulse, but in multiple distinct frequency bands. This technique adds another discriminatory dimension to the problem and yields superior results. In the frequency domain, PDs of different types can be effectively characterized for localization. Most of the frequency domain methods used in PD signal analysis and localization are based on the well-known Fast Fourier transform (FFT) techniques [16], [19]. However, PD signals are stochastic and often demonstrate a nonstationary and transient nature, carrying small yet informative components embedded in larger repetitive signals [1]. This limits the application of FFT based techniques for PD localization.

In this work, a low cost approach, which uses the Wavelet Transform [20] to decompose RF PD signals into different frequency bands and extract PD location dependent parameters for robust PD localization is presented and evaluated in this paper. A machine learning ensemble technique is employed for improved PD localization.

II. FEATURE EXTRACTION

Feature extraction is one of the necessary preprocessing steps of machine learning and pattern matching [21]. Its aim is to extract the most informative inputs (features) from raw PD signals. Good features are highly correlated with the expected outputs but have low correlation with each other. The extracted features facilitate the subsequent learning and generalization steps, and in some cases, lead to better interpretations.

Partial discharge (PD) RF pulses collected during the measurement campaign are corrupted by noise due to external disturbances. Extracting PD pulses from such noisy measurements is therefore crucial. It is also important that this is done in such a way that the features of the PD pulse are preserved as much as possible. In this work, a multivariate de-noising method [22]–[24] that combines wavelets and Principal Component Analysis (PCA) is applied to the PD data in order to isolate the PD signals from noise without assuming any *a priori* knowledge of the PD features. This technique combines the decomposition of information given by the wavelet transform with the

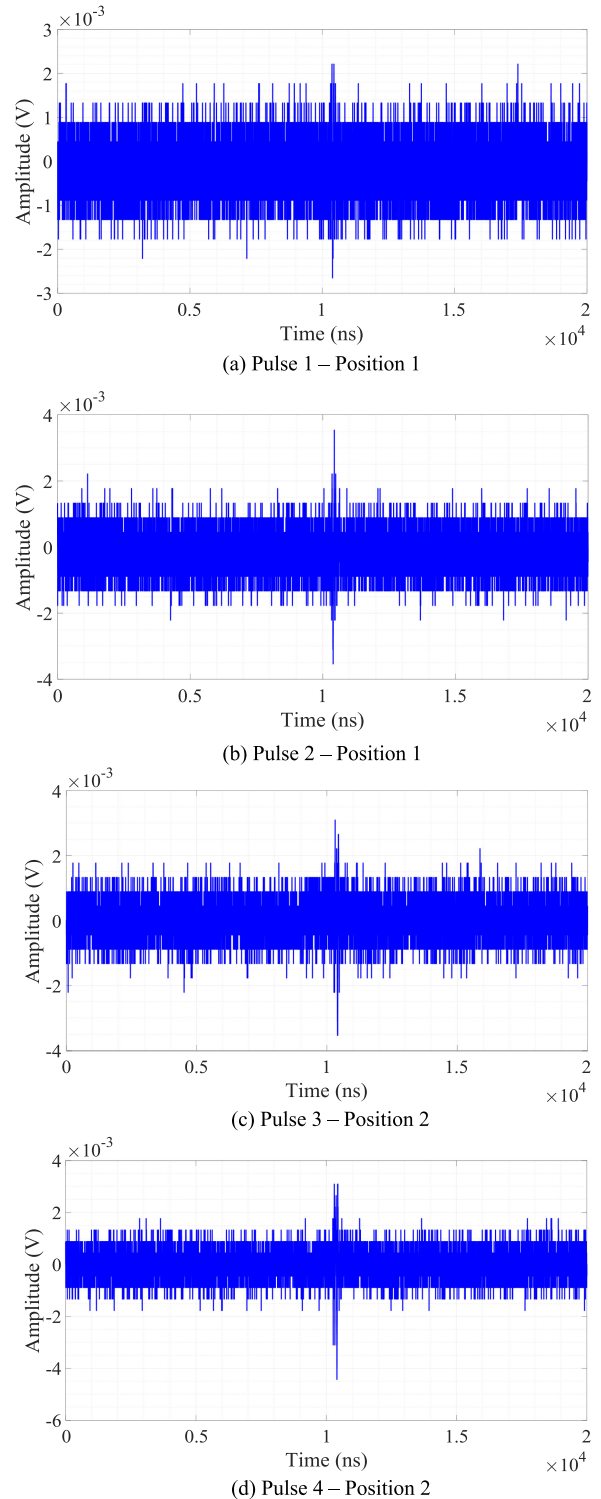


Fig. 1. Emulated PD pulse with noise.

ability to orthogonalize variables provided by PCA. The objective is to obtain de-noised PD data so as to extract meaningful information for PD location. Samples of noise corrupted PD signals recorded are as shown in Fig. 1. PCA here is not used to discover new variables which could be of interest, but to take advantage of the deterministic links among the signals, offering

an additional de-noising layer by omitting insignificant principal components. In parallel, PCA is performed on the wavelet approximation coefficients to keep the most important features of the PD signals. Kaiser's rule [25] is used to automatically select the minimum numbers of retained principal components (components associated with eigenvalues exceeding the mean of all eigenvalues). The Daubechies wavelet db14 with a 5th level decomposition which has been used for PD de-noising [26] is adopted in this work. Owing to the fact that only a few of the wavelet coefficients describing PD waveform carry significant information, hard-thresholding is employed. The PD de-noised signal samples are shown in Fig. 2.

A. Wavelet Transform

The application of wavelet transformation in PD signal analysis is a well-known technique which overcomes the problems of other signal processing techniques such as the Fourier Transform which can describe the frequency components contained within a complex signal, but cannot indicate where in time those frequencies reside. A wavelet-based approach permits isolation and extraction of energies in both time and frequency. In any complex radio environment, such as a substation, multipath propagation will occur as a result of reflection and diffraction from various obstacles and structures; this gives rise to many delayed and attenuated versions of the emitted PD pulse. The superposition of these received pulses produces a temporal signature (energy versus time) from which higher order features can be extracted. The shape of the pulse in the time-domain will be dependent on the location of the source. Multipath effects are also known to be frequency-selective in that the shape of the signature will change based on the frequency of the pulse. Thus, the aggregated PD pulse as seen by the receiver can be effectively band-pass filtered to produce distinct time-energy signatures in each band. In doing so, we can exploit the frequency-selective nature of multipath propagation to generate more distinct features to aid the localization algorithm. This filtering process is achieved via a wavelet-based approach as follows.

Unlike spectral analysis that represents a signal as a sum of sinusoidal functions, the wavelet transform decomposes the signal into wavelets of various scales in the time-domain with variable window sizes thus revealing the local structure in the time-frequency domain. The continuous wavelet transform [27] of a signal $s(t)$, is given as:

$$W_s(a, b) = \frac{1}{\sqrt{a}} \int_{-\infty}^{+\infty} s(t) \psi^* \left(\frac{t-a}{b} \right) dt, \quad (1)$$

where $\psi(t)$ is the mother wavelet, a and b are the scale and shift parameters respectively. The computational burden involved in computing the many coefficients generated by continuous wavelet transform for every scale and time is overwhelming. An efficient alternative is to discretize a and b by replacing $a = 2^{-j}$ and $b = k2^{-j}$, where k and j are integers. This forms the discrete version of wavelet transform. This is expressed as:

$$W_s(j, k) = \int_{-\infty}^{+\infty} s(t) 2^{j/2} \psi_{j,k}^* (2^j t - k) dt, \quad (2)$$

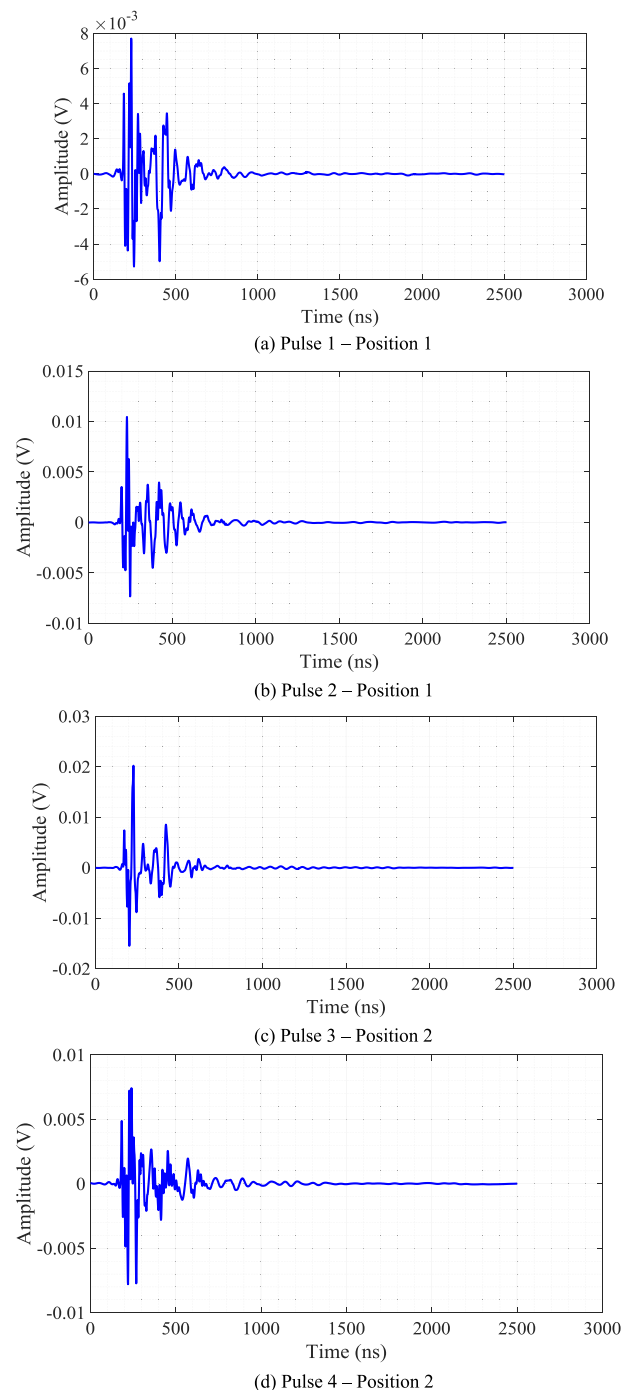


Fig. 2. De-noised PD pulses.

The Discrete Wavelet Transform (DWT), which is one of the popular methods in the wavelet transformation family has been widely used in PD signal processing, classification and de-noising [20], [28]–[31]. The DWT uses a cascade of low and high pass filters to decompose the PD signal into two components: detail coefficients (DCs), which contain the high frequency, low scale information of the PD signal and approximation coefficients (ACs), which capture the low frequency, high scale information of the PD signal. While the DCs remain unchanged at

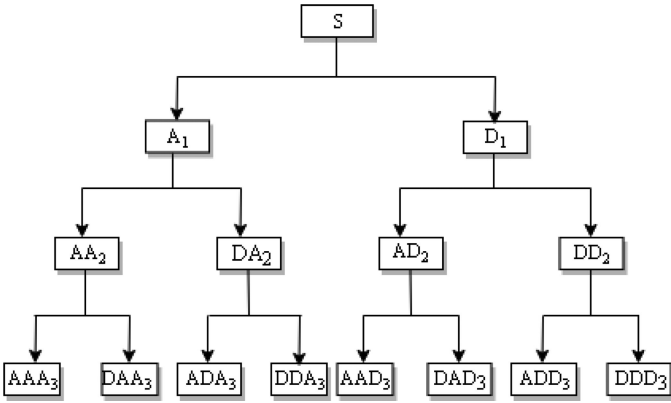


Fig. 3. General architecture of the WPT.

each level of decomposition, the ACs are further decomposed into DC and AC subsets. This process continues until the final decomposition level [32]. In this way, DWT decomposes PD signals into different scales, generating multi-scale features which reveal the local features of the PD signals. However, with DWT some intrinsic characteristics of the signals in the high frequency region are still buried in the DCs since only ACs are decomposed in each level.

B. Wavelet Packet Transform

The Wavelet Packet Transform (WPT) [33]–[35] is viewed as an extension of the DWT providing a level by level transformation of a signal from the time domain to the frequency domain. The top or first level of the WPT is the time representation of the PD signal. At every other level down the WP decomposition tree, there is a decrease in temporal resolution and a corresponding increase in frequency resolution. This helps capture the high frequency information in the PD signals which are not normally represented in DWT.

In other words, unlike the DWT, the WPT decomposes both the DCs and the ACs simultaneously at every level. Therefore, the WPT has the same frequency bandwidth in each resolution. This enables the WPT to preserve the information in the original PD signals, resulting in robust features. The general architecture of the WPT decomposition is shown in Fig. 3. The tree is typically a binary tree, where each node has both DCs (right sub-node) and ACs (left sub-node). In practice, WPT decomposition is achieved via a quadrature mirror filter pair (low-pass and high-pass). Let the wavelet packet function be given by:

$$V_{j,k}^n(t) = 2^{j/2} V^n(2^j t - k) \quad (3)$$

where j is a scaling parameter, k and n are a translation and oscillation parameters respectively. And the scaling and wavelet function represented by $\phi(t)$ and $\psi(t)$ respectively, then the wavelet filters can be constructed using the following expression [36]:

$$\phi(t) = \sqrt{2} \sum_k g_l \phi(2t - k) \quad (4)$$

$$\psi(t) = \sqrt{2} \sum_k g_h \psi(2t - k) \quad (5)$$

where g_l and g_h are the low-pass and the high-pass filters respectively. The scaling and wavelet functions are equivalent to the first two wavelet packet functions given as:

$$V_{0,0}^0(t) = \phi(t) \quad (6)$$

$$V_{0,0}^1(t) = \psi(t) \quad (7)$$

This implies that for $n = 0, 1, 2, \dots$, the wavelet packet functions can be expressed as:

$$V_{j,k}^{2n}(t) = \sqrt{2} \sum_k g_l V_{j-1,k}^n(2t - k) \quad (8)$$

$$V_{j,k}^{2n+1}(t) = \sqrt{2} \sum_k g_h V_{j-1,k}^n(2t - k) \quad (9)$$

Therefore, features can be extracted from both DCs and ACs at different levels to obtain valuable information. In [37], the WPT was used to decompose PD signals into multiple scales, and extract PD features for PD classification. In this work, WPT is used for locating PD sources.

C. Feature Extraction of PD Signals Using WPT

The Wavelet Packet Transform is introduced as an alternative method of extracting the desired location dependent features from PD signals. First, the PD data is decomposed via the WPT to extract the time-frequency-dependent information. Thus sequenced-ordered wavelet packet coefficients for the wavelet packet transform nodes at each level of decomposition are obtained. The standard choice for depth of decomposition level is specified as a positive integer: 4 or floor($\log_2(\text{length}(\text{signal}))$), whichever is smaller [37]. In our case, the transform level is set to 4 since the signal is long. The 4-level WPT decomposition generates a tree with 16 terminal nodes, corresponding to the frequency sub-bands. Features are defined based on the wavelet packet node coefficients. For any function f , the wavelet packet coefficient is given by:

$$v_{j,n,k}(t) = \langle f, V_{j,k}^n \rangle = \left\langle f, 2^{j/2} V^n(2^j t - k) \right\rangle \quad (10)$$

Each $v_{j,n,k}$ coefficient measures a specific sub-band frequency content, controlled by the scaling parameter j and the oscillation parameter n , of a signal around the time instant $2^j t$. Unlike discrete wavelet transform, the filtering operations in wavelet packet transform, are also applied to the wavelet, or detail coefficients. The frequency-localised filter; Fejer-Korovkin wavelet has been shown to be a good approximation [38]. The result is that wavelet packets provide a sub-band filtering of the input signal into progressively finer equal-width intervals. At each level j , the frequency axis is divided into 2^j sub-bands. The sub-bands in Hertz at level j are approximately

$$\left[\frac{n f_s}{2^{j+1}}, \frac{(n+1) f_s}{2^{j+1}} \right) \quad (11)$$

where $n = 0, 1, \dots, 2^j - 1$ and f_s is the sampling frequency.

The wavelet packets have the added benefit of being an orthogonal transform, which means the energy in the signal is preserved and partitioned among the sub-bands as mentioned

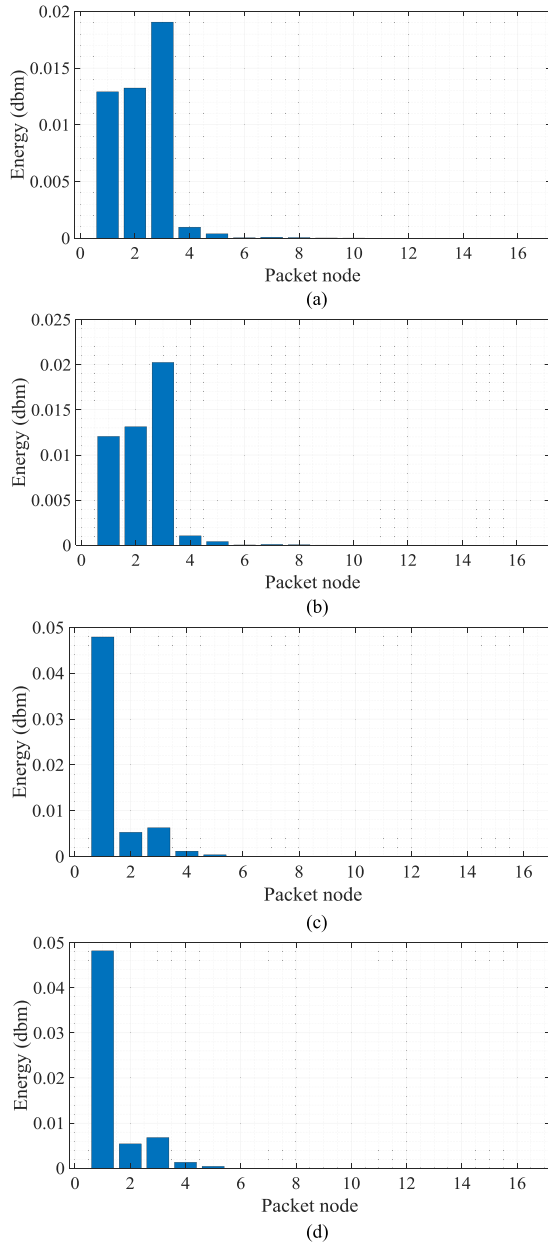


Fig. 4. PD wavelet packet node energy distribution for the 4 de-noised pulses in Fig. 2. (a) Pulse 1-position 1. (b) Pulse 2-position 1. (c) Pulse 3-position 2. (d) Pulse 4-position 2.

earlier. Therefore, the wavelet packet node energy can represent the characteristics of PD signals, and it is defined as

$$e_{j,n} = \sum_k v_{j,n,k}^2 \quad (12)$$

This measures the PD signal energy contained in each sub-band indexed by parameters j and n . Here, we refer to each (j, n) as a wavelet packet node. The sum of the energy over all the packets nodes equals the total energy of the signal. $e_{j,n}$ can be normalized over the total energy, representing the energy of each packet. However, in this work, our interest is in the sub-band energy. As an illustration, Fig. 4 depicts the energy

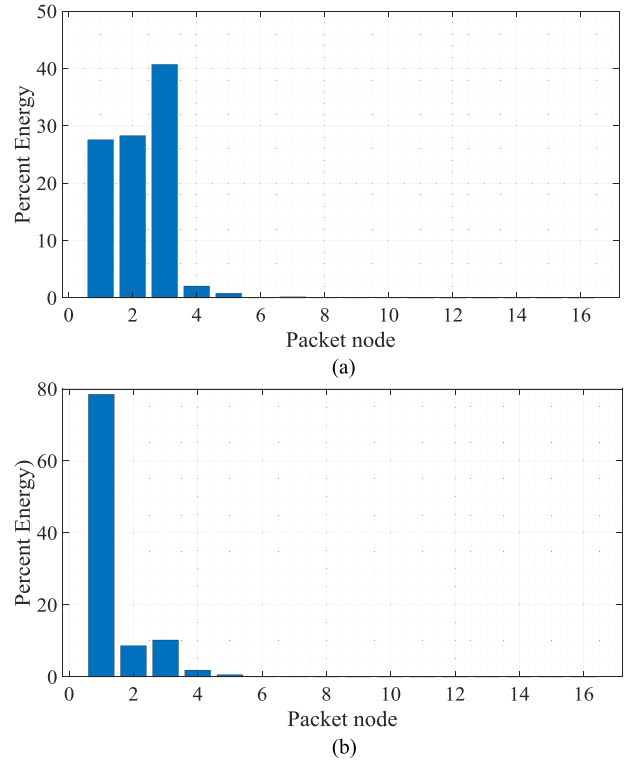


Fig. 5. Normalized signal energy by node for (a) signals in Fig. 4(a)/(b) and (b) signals in Fig. 4(c)/(d).

distribution computed based on all coefficients in each wavelet packet node for four de-noised PD signals represented in Fig. 2. Fig. 2 shows the temporal signature of four distinct PD pulses at two different locations. And will be explained more fully in Section III. Specifically, Fig. 4 *a/b* depicts the energy profile of two distinct pulses transmitted from the same location (location 1), and Fig. 4 *c/d* depicts the energy profile of another two pulses transmitted from a second location (location 2). By examination of packet nodes 1 to 3 (first three bars in Fig. 4), it is evident that subplots *a* and *b* are very similar, these are distinct signals from the same location. Likewise, subplots *c* and *d* are very similar, these represent two distinct pulses from a second location. However, the signals from *a* or *b* are distinct from those of *c* or *d*. Thus, the wavelet packet node energy distribution represents an excellent set of features for PD localization because it is (i) time invariant, and (ii) location dependent. It is important to identify the frequency bands that contain most of the PD pulse energy. PD signals are known to have a very short duration (nanosecond), which implies a high frequency content. However, there are always dominant frequency bands that contain greater pulse energy in the entire spectrum. The relative energy by node shown in Fig. 5 reveals the nodes with higher percentage of pulse energy, indicating 3 frequency passbands of interest. The resulting passbands emphasize frequencies between 62.5–250 MHz, which contains large portions of the PD signal energy. The lower and upper frequencies of each wavelet packet frequency band are presented in Table I. In the presence of noise the PD energy will be buried in noise in some frequency

TABLE I
WPT-BASED EXTRACTED PD FREQUENCY BANDS

	Lower frequency	Upper frequency
BAND 1	62.5 MHz	125 MHz
BAND 2	125 MHz	187.5 MHz
BAND 3	187.5 MHz	250 MHz

bands making it a challenge to find where PDs lie. The significant advantage of the proposed WPT technique lies in its ability to identify these frequency bands even in noisy PD signals. Given noisy PD signals as shown in Fig. 1, it has been demonstrated that the wavelet packet transform identifies the frequency bands with most of the PD pulse energy as wavelet packet nodes at the terminal level using (12). The energy distribution of these noisy signals in the frequency bands after transformation is as shown in Fig. 6. This demonstrates the robustness of the proposed technique in the presence of noise. In this work, each node energy equivalent to energy in a frequency passband, represents an individual PD feature component.

This work is based on the assumption that all PD features extracted using the WPT provide meaningful information for inferring the PD location. To demonstrate that this is a reasonable assumption, Fig. 7(a-c) shows how the maps of the PD features at each of the 3 antennas vary with location. The effect of multipath and signal distortions add to the unique signature created at different locations.

III. EXPERIMENTAL PROCEDURE

In order to evaluate the feasibility of using the WPT-based frequency domain PD features in conjunction with machine learning ensembles to locate a PD source, an experiment was conducted in the laboratory at the University of Strathclyde with approximate dimensions of 19.2 m \times 8.4 m. This environment is characterized by multipath propagation which is a result of cluttered objects including metallic ones. Although the radio environment within the laboratory cannot be expected to approximate that within an electrical substation, it is sufficiently complex to enable evaluation of the PD localisation techniques being investigated. The floor map is shown in Fig. 8. On the map, three receiver sensors indicated by antennas are positioned at random with considerable distance between them whereas reference (training) and test locations represented as (blue) circles and (red) diamond marks respectively are defined on a grid. These training and test locations simulate PD sources and are so called given that they represent different sets of data to be used in this work. At every training and test location, PD emulated signals are generated and recorded. A pulse signal generator was used to emulate PD signals in this experiment. The pulse generator is capable of generating sub-nanosecond current pulse which was fed to a monopole antenna. The radiating monopole antenna therefore represents an artificial PD source. Commercial-off-the-shelf Omni-directional antennas operating at 173 MHz were used to capture the generated PD signals. The frequency response of the antennas is depicted in Fig. 9.

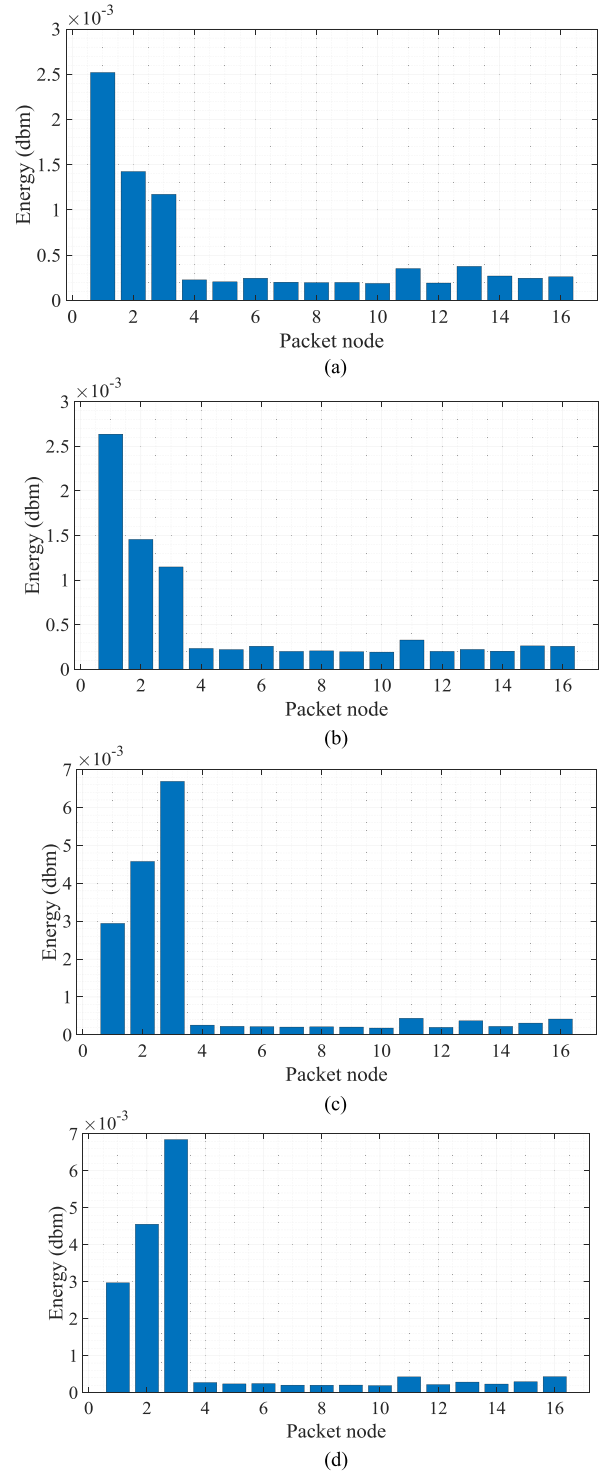


Fig. 6. PD wavelet packet node energy distribution for the four noisy pulses in Fig. 1. (a) Pulse 1-position 1. (b) Pulse 2-position 1. (c) Pulse 3-position 2. (d) Pulse 4-position 2.

These sensors were connected to a multichannel digital oscilloscope where the PD pulse traces were recorded for further analysis. 20 samples of PD signals were generated and collected for each of the 144 reference (training) locations (blue circles)

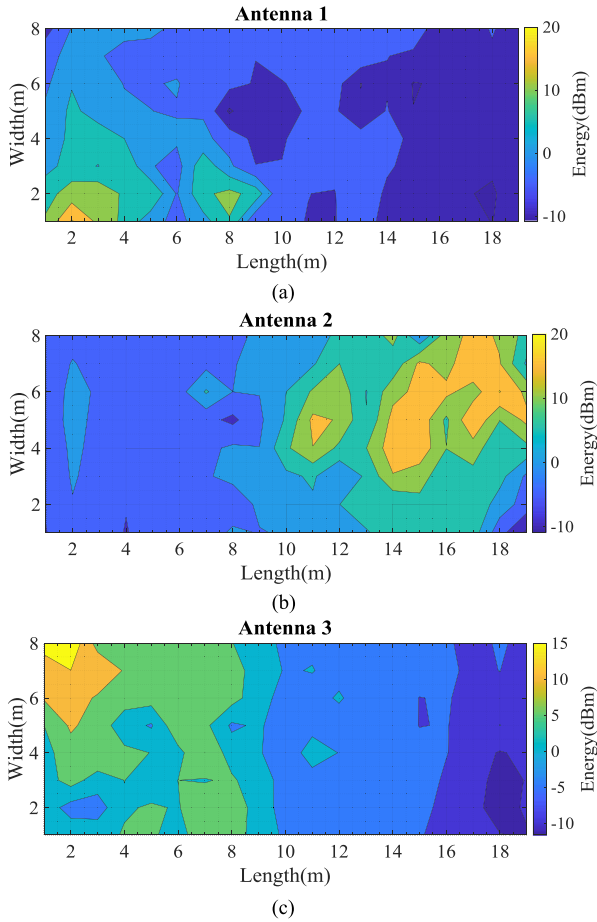


Fig. 7. Spatial representation of WPT-based PD energy in band 1.

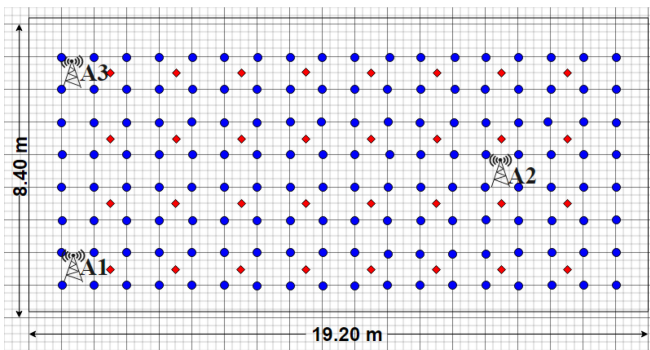


Fig. 8. PD measurement grid.

to build a training database. The training points were separated by 1 m on a uniform grid. For testing the PD localization scheme developed in this paper, 20 PD signal measurements were collected at each of the 32 distinct test locations (red diamonds) on the same grid in Fig. 8. The spacing between the test points is 2.5 m. This setup ensures that the 20×144 training and 20×32 testing samples are disjoint enough to provide realistic results. A sample of the PD emulated pulse and the received pulse captured by the sensors is as shown in Fig. 10.

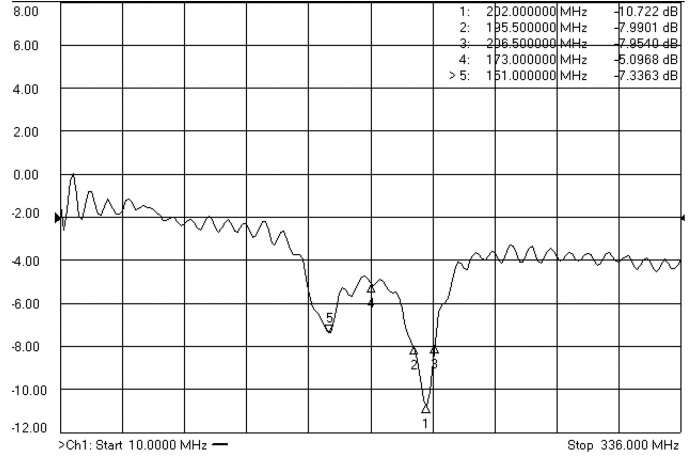


Fig. 9. Antenna frequency response.

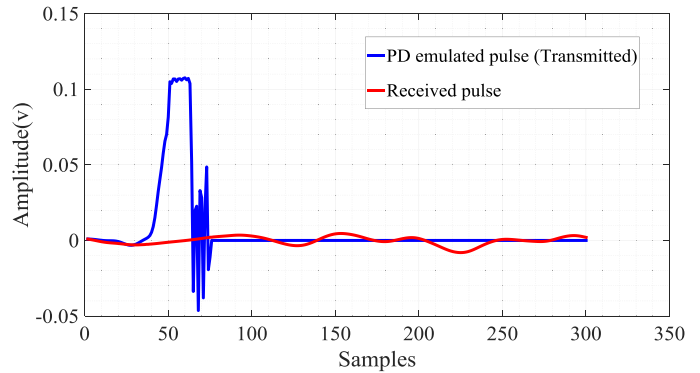


Fig. 10. Response of the receiver sensor and the emulated PD pulse.

IV. MACHINE LEARNING-BASED PD LOCALIZATION METHODS

A. Regression Tree-Based PD Localization Method

The Regression Tree is one of the most efficient machine learning algorithms used for predictions [39]–[41]. It is considered a variant of a binary decision tree model composed of linear regression functions at the leaf nodes. In this work, it is designed to learn and approximate the nonlinear function (PD locations/WPT-based PD features) by piecewise linear functions at the leaf nodes. In other words, the nonlinear mapping of PD features to PD location coordinates is handled by splitting the problem into a set of smaller problems addressed with simple linear predictors. Fig. 11 shows the architecture of a regression tree. Each node in the tree is designed to split the data so as to form clusters where accurate predictions can be performed with simple models. During training, a PD regression tree model is built top-down from the root node through binary recursive partitioning, which is an iterative process that splits the PD training data (PD features/location) into subsets that contain features with similar values. The parameters of the tree such as number of splits are optimized during training. A sum of squares reduction criterion is used in partitioning the data.

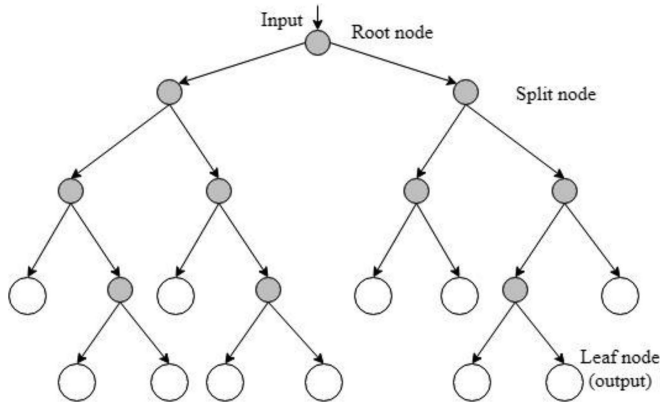


Fig. 11. General architecture of a regression tree.

The algorithm selects the split at each node that minimizes;

$$SS = \sum_R ((x, y)_i - (x, y)_R)^2 + \sum_L ((x, y)_i - (x, y)_L)^2 \quad (13)$$

where $(x, y)_R$ and $(x, y)_L$ are the estimated values for the right and left nodes respectively. This process continues until it reaches the terminal (leaf) node. The terminal nodes of the tree which represents a cell of the partition, store the models that approximate the best desired output. Suppose the training points at the terminal node are $(r_i, (x, y)_i), (r_2, (x, y)_i), \dots (r_n, (x, y)_n)$, then the local model for the terminal node is

$$(\hat{x}, \hat{y}) = \frac{1}{n} \sum_{i=1}^n (x, y)_i \quad (14)$$

In the localization phase, the location coordinate of any PD sample (features) can be estimated by following through the branches of the obtained tree model. Despite the simplicity that comes with the implementation of regression trees, the issue of overfitting affects its performance. When fully grown, it may lose some generalization capability.

B. Bootstrap Aggregating Method for PD Localization

Bootstrap aggregating [42]–[44], also known as bagging is a machine learning ensemble algorithm that combines a multitude of decision trees in order to improve performance. For PD localization, bagging is used to model the non-linear relationship between WPT-PD features and PD location. Instead of growing a single tree from the complete data set during training, bagging grows many trees using bootstrap (equiprobable sampling with replacement) samples of the PD data. Each sample is different from the original data set, yet resembles it in distribution and variability as a result of random sampling. Different tree models are grown for each bootstrap sample. Mathematically, given a training input set $R = r_1, \dots, r_n$ and corresponding training output set $(X, Y) = (x, y)_i, \dots, (x, y)_n$, bagging repeatedly (M times) selects subsets (randomly sample with replacement) of these training set and builds trees with each subset. For $m = 1, \dots, M$: bagging builds t_m models. After

training, the location estimate for unseen sample r' can be taken as the average estimates of all the individual tree models on r' given as;

$$\hat{t} = \frac{1}{M} \sum_{m=1}^M t_m(r') \quad (15)$$

The performance of bagging is affected by the particular bootstrap sample size used. Therefore, Bayesian optimization is used to tune the model parameters. PD location is then determined by taking the average of the outputs from all the trees. Random sampling helps overcome the problem of overfitting in regression trees and improves predictions. However, there exist high correlations in prediction among some of the PD localization subtrees, limiting the performance of the bagging regression trees. This motivates the use of a robust PD localization algorithm: random forest.

C. Random Regression Forest PD Localization Method

Random Regression Forest (RRF) is an ensemble of different regression trees widely used in prediction [45]–[47]. The main idea of RRF is to grow many regression trees based on some randomly selected features (sub-spacing) from randomly selected samples with bootstrap strategy. In the context of PD localization, each tree is regarded as a function approximation problem consisting of a non-linear mapping of the PD input features onto the x-y coordinates representing PD location. The nonlinearity is achieved by dividing up the original PD localization problem into smaller ones, solvable with simple models. A multivariate RRF model is developed to locate PD source to its x and y coordinate.

The RRF-PD localization technique consists of two phases: a training phase and a location estimation phase. In the training phase, RRF grows multiple regression trees from bootstrap samples of the training data. Each sample subset comprises PD features and associated ground-truth locations. At each split or node, only a random subset of the PD features is considered. The size of the forest is fixed and all the trees are trained in parallel. During training, the parameters of the model are optimized.

In the location estimation phase, each previously unseen PD features sample is given as an input to each tree in the forest starting at the root and the corresponding sequence of tests applied. Each tree gives an estimate of the location coordinate and the final prediction is taken as the average of the trees predictions. The flowchart of the RRF framework is as shown in Fig. 12. The selection of random samples of features at each split produces uncorrelated subtree predictions. Combining multiple decorrelated PD-tree models increases robustness to variance and reduces overall sensitivity to noise. This is demonstrated by the results obtained.

V. LOCALIZATION RESULTS AND DISCUSSION

This section provides empirical evaluation of the performance of the PD localization methods described in Section III. The PD data used for testing is taken from a set of 32 different grid

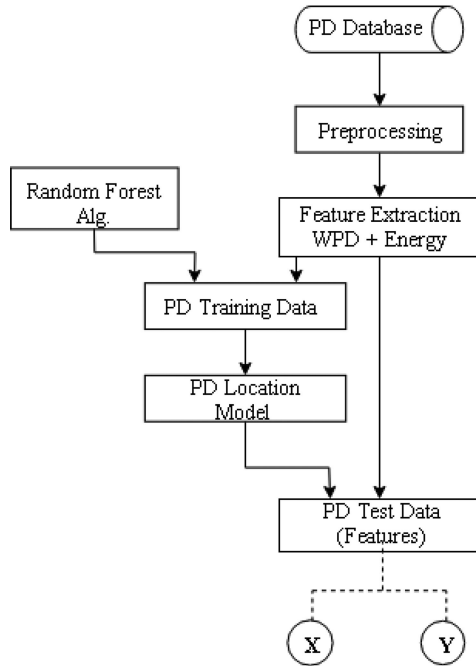


Fig. 12. Flowchart for Random Forest PD Localization.

locations, independent of the training set, but obtained with the same procedure.

A. Evaluating Localization Accuracy

Localization errors for each PD location model developed are shown in Table II. The x and y coordinate error columns represent the error in the x and y direction respectively, however, these columns may not correspond to the same physical location. For example, for RT-best the x-error is 0 for one location but has a non-zero y value. Similarly, for a different location y is 0 but has a non-zero error. Errors in x and y coordinates are defined as absolute differences between predicted and true locations. Column 3 represents the overall localization error (Euclidean distance between the predicted and true locations). Despite the data variability and the area covered, a mean error of 1.9 m obtained is sufficient for PD location. The models are trained on 2880 PD data measurements and tested on 640 PD data measurements. The normalized WPT-based features extracted from the 2880 measurements with corresponding locations are used as input to the models for training. The maximum number of PD features used at each split is 1/3 of the total number of features. In this work, 1000 trees are grown. This optimal number is estimated internally during the computations.

Fig. 13 shows the estimated PD source location (red diamond) with the lowest localization error for each model using WPT-based features. The blue dot represents the actual PD source position. The black squares represent emulated sensor node positions. The results show that the minimum location error is superior when ensemble methods are applied on the WPT-based features. Regression tree can locate the exact x or y coordinates with zero error in some instances as shown in Table II but fails

TABLE II
STATISTICS OF PD LOCATION ERROR FOR EACH METHOD

PD Location Method	X-coordinate error (m)	Y-coordinate error (m)	Location Error (m)
Reg. Tree (best)	0.0000	0.0000	0.5000
Reg. Tree (worst)	8.5000	6.5000	8.9253
Reg. Tree (mean)	1.3712	1.9808	2.7017
Reg. Tree (variance)	2.0257	2.8912	3.4191
Bootstrap (best)	0.0020	0.0029	0.0829
Bootstrap (worst)	5.6550	6.0736	6.2197
Bootstrap (mean)	0.9452	1.5213	1.9839
Bootstrap (variance)	0.5786	1.7839	1.6330
RRF (best)	0.0031	0.0021	0.0789
RRF (worst)	5.1260	5.7435	6.0531
RRF (mean)	1.0019	1.4296	1.9152
RRF (variance)	0.5512	1.4633	1.3930

to provide a robust model, with worst location error as high as 8.9 m. This is shown in Fig. 14.

Fig. 15 further illustrates the difference in accuracy among the three models by comparing the cumulative density functions (CDFs) of location errors. It can be observed that random forest increased the overall confidence probability of errors within 3 m to 91% which is significantly larger than the probability of 70% achieved by regression tree. This is however unsurprising as the regression tree is a weak learner. Random forest has also reduced the mean of location errors by 29% compared to regression tree. Given that the spacing between test locations is 2.5 m, the proportion of test data with a localization error below this value is also evaluated. For the regression tree method, 68% of test points were below 2.5 m. For the bagging algorithm, 75% are below, and for the random forest 78% are below.

B. Evaluating Model Robustness

Another key aspect of the proposed PD location scheme is its robustness. By comparing the location accuracy in x and y coordinates and the overall precision, the ensemble methods provide more robust models for PD localization. Furthermore, Fig. 16 shows the variance in location error of the models using training and testing datasets. Random forest, in particular, showed a much lower variance between training and testing predictions, making it more robust compared to regression tree and bootstrap aggregating models. Fig. 17 shows PD localization results from 3 random locations. Each discrete point corresponds to a single location estimate of a radio measurement. Also shown for the three PD localization models is the confidence ellipse that contains 95% of the estimates for each location. For point (2.5, 1.5) the regression tree estimates fall on a straight line. This means that the covariance in the y-direction is zero. Therefore, the width of the ellipse is zero in that direction. The size of the ellipse is an indication of the precision of the estimate. Random forest shows a more precise estimate with a smaller confidence ellipse. The large ellipses of Regression Tree indicates a less

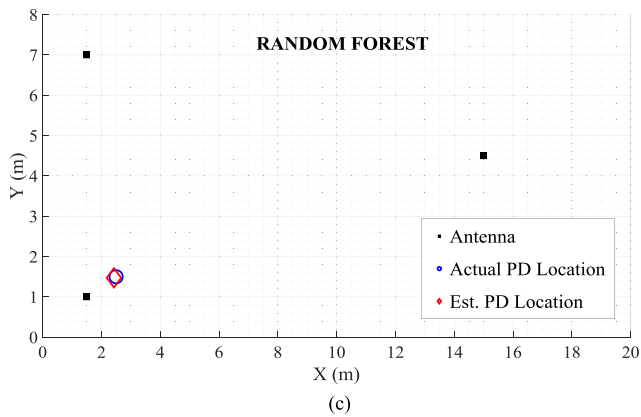
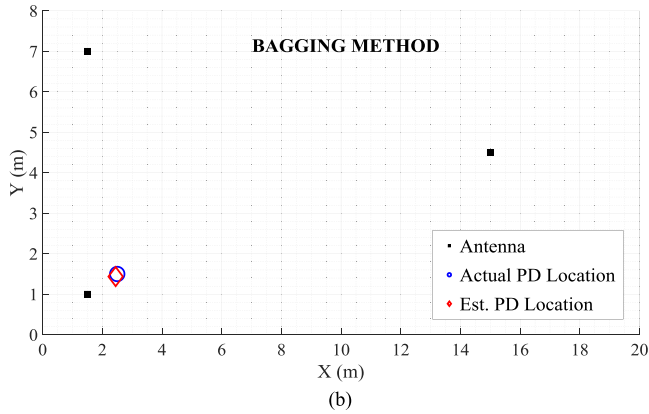
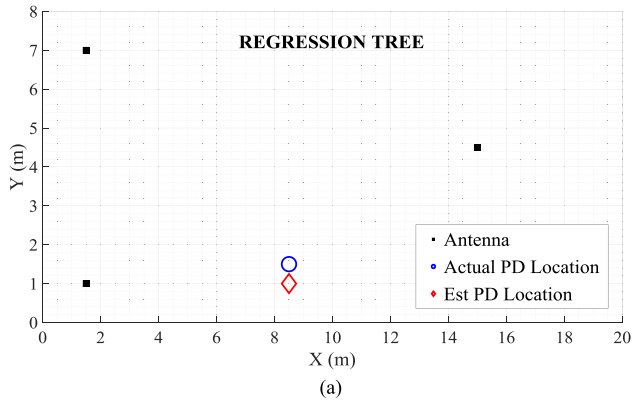


Fig. 13. PD best location estimates. (a) Random Forest. (b) Bagging. (c) Regression tree.

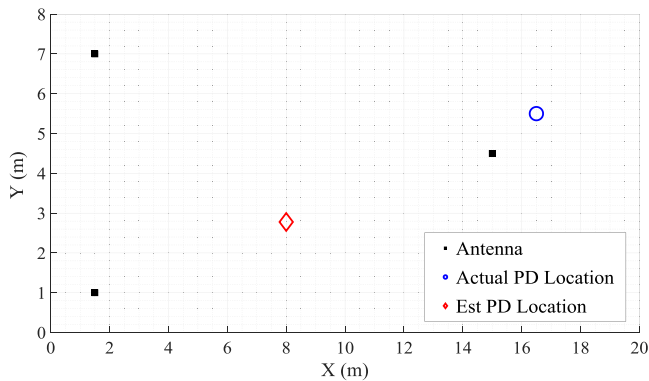


Fig. 14. Regression tree PD worst location estimate.

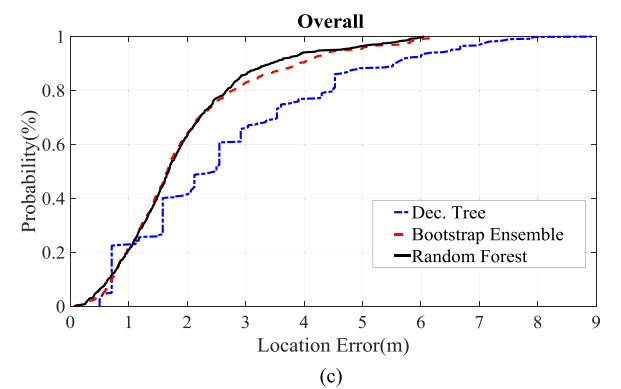
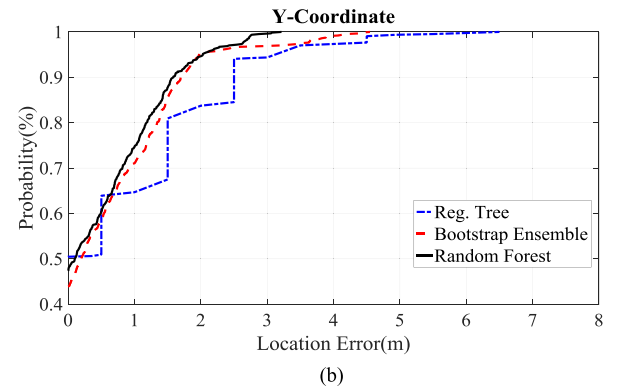
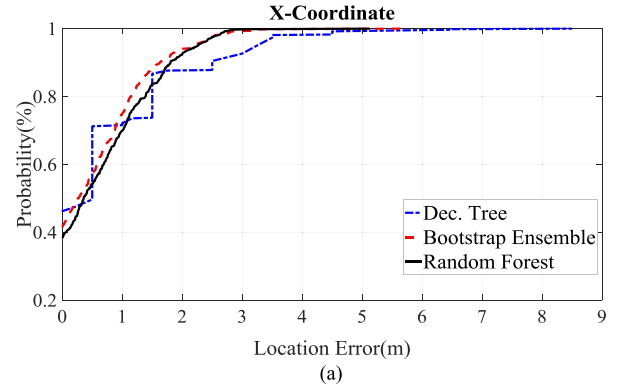


Fig. 15. CDF of location errors in (a) x-coordinate, (b) –coordinate, (c) overall.

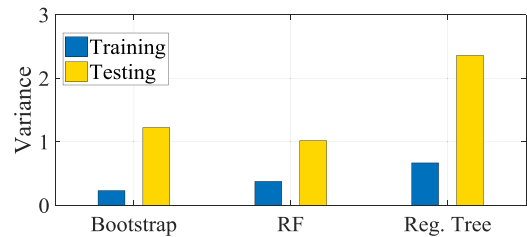


Fig. 16. Variance of location error.

precise location estimate. This further demonstrates the robustness of the proposed WPT-based Random Forest PD localization scheme.

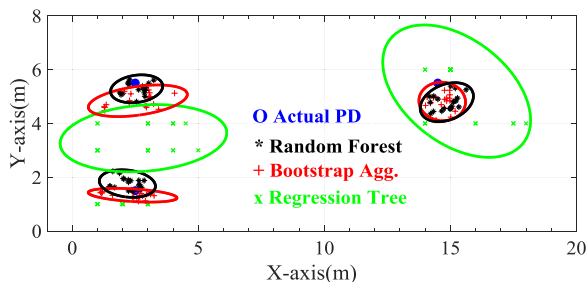


Fig. 17. PD location results for 3 different points.

C. Comparison With Related Works

There are other substation-wide PD localization schemes in literature that are worth comparing with our proposed solution. In [48], the authors developed a Software Defined Radio (SDR) PD localization system based on received signal strength to infer PD location. However, they presented results for a single location estimate which we assumed to be the best location estimate; this approach yielded a location error of 1.3 m. Another RSS-based PD localization system was proposed in [49]. Here, the system involves estimating the path loss exponent and converting the RSS into distance. Two scenarios were created in terms of the number of receiving sensors used for capturing PD signals; seven sensors for scenario 1 and eight sensors for scenario 2. The test site was an 18 m \times 18 m empty room. For the nine test locations, the best estimated location error for scenario 1 and scenario 2 are 0.78 and 1.06 m respectively. In another work [50], a PD localization scheme based on RSS fingerprint was proposed for a 24 m² test bed with grid spacing of 1 m \times 1 m. The localization phase includes two stages of processing: a preliminary localization stage where particle swarm optimization and back propagation neural network are used, and a more accurate localization stage where compressive sensing is employed for accurate localization. Their result shows an average localization error of 0.89 m with maximum error 3.61 m. However, this result comes at an extra cost of two stages of computation in the localization phase. A probability based technique for PD source localization was proposed in [51]. Time difference of arrival (TDoA) was used as PD feature. A test of three PD sources was carried out and the result indicates localization errors of 0.56 m, 1.59 m and 0.18 m for the three sources. In [52], an automated system for PD detection and localization based on Gaussian mixture model was presented. Time delay of arrival was used to locate PD sources. This work presented result for eight location estimate with minimum error of 0.5 m and an average location error of 1.4 m. Authors in [53] proposed an RSS-based PD localization method to locate power equipment in substation with potential insulation defect. This involves two stages of localization: a preliminary localization by cluster recognition and compressed sensing algorithm. The test site used for this experiment measured 24 m \times 24 m with 625 grid points (1 m \times 1 m). Their result indicates that the proportion of estimated location errors within 3m is 89.6%. Our proposed solution, WPT-based RRF PD localization scheme is a simple and low-cost solution

for PD localization with best estimated location error of 0.31 m. Our result also indicates that 91% of the PD sources were located with error less than 3 m.

VI. CONCLUSION

A robust PD localization scheme based on the wavelet packet transform and the ensemble learning method has been considered. The scheme utilizes the PD measurements captured with sensors placed in the vicinity of the discharge source, as follows.

- 1) The measured PD signals are first decomposed using WPT decomposition to extract PD location dependent features. The WPT selects the frequency bands with equal bandwidth where the energy of the noisy PD signal is concentrated through a transformation such that the retained signal information is maximized in order to ensure high accuracy.
- 2) The WPT-based PD features are then used to build the ensemble models.
- 3) PD location is obtained via a multivariate regression forest algorithm which provides a more robust and accurate approach compared to regression tree and bootstrap aggregating methods.

In this study, regression forest increased the overall confidence probability of errors within 3 m to 91% compared to 70% achieved by regression tree; an improved accuracy of 29%. The results suggest that the proposed PD localization method described in this paper represents a practical approach to PD localization. The simplicity and robustness of the technique makes it worth considering in future implementations of the smart grid.

REFERENCES

- [1] J. C. Hernandez-Mejia, J. Perkel, R. Harley, M. Begovic, R. N. Hampton, and R. Hartlein, "Determining routes for the analysis of partial discharge signals derived from the field," *IEEE Trans. Dielect. Elect. Insul.*, vol. 15, no. 6, pp. 1517–1525, Dec. 2008.
- [2] X. Peng, C. Zhou, D. M. Hepburn, M. D. Judd, and W. H. Siew, "Application of K-Means method to pattern recognition in on-line cable partial discharge monitoring," *IEEE Trans. Dielect. Elect. Insul.*, vol. 20, no. 3, pp. 754–761, Jun. 2013.
- [3] H. A. Illias, M. A. Tunio, A. H. A. Bakar, H. Mokhlis, and G. Chen, "Partial discharge phenomena within an artificial void in cable insulation geometry: Experimental validation and simulation," *IEEE Trans. Dielect. Elect. Insul.*, vol. 23, no. 1, pp. 451–459, Feb. 2016.
- [4] J. Li, X. Han, Z. Liu, X. Yao, and Y. Li, "PD characteristics of oil-pressboard insulation under ac and dc mixed voltage," *IEEE Trans. Dielect. Elect. Insul.*, vol. 23, no. 1, pp. 444–450, Feb. 2016.
- [5] H. Hou, G. Sheng, and X. Jiang, "Localization algorithm for the PD source in substation based on L-shaped antenna array signal processing," *IEEE Trans. Power Del.*, vol. 30, no. 1, pp. 472–479, Feb. 2015.
- [6] M. Yoshida, H. Kojima, N. Hayakawa, F. Endo, and H. Okubo, "Evaluation of UHF method for partial discharge measurement by simultaneous observation of UHF signal and current pulse waveforms," *IEEE Trans. Dielect. Elect. Insul.*, vol. 18, no. 2, pp. 425–431, Apr. 2011.
- [7] M. X. Zhu *et al.*, "Localization of multiple partial discharge sources in air-insulated substation using probability-based algorithm," *IEEE Trans. Dielect. Elect. Insul.*, vol. 24, no. 1, pp. 157–166, Feb. 2017.
- [8] H. H. Sinaga, B. T. Phung, and T. R. Blackburn, "Partial discharge localization in transformers using UHF detection method," *IEEE Trans. Dielect. Elect. Insul.*, vol. 19, no. 6, pp. 1891–1900, Dec. 2012.
- [9] I. Portugues, P. J. Moore, and I. A. Glover, "Characterisation of radio frequency interference from high voltage electricity supply equipment," in *Proc. 12th Int. Conf. Antennas Propag.*, Exeter, U.K., 2003, pp. 820–823.

- [10] I. E. Portugues, P. J. Moore, and P. Carder, "The use of radiometric partial discharge location equipment in distribution substations," in *Proc. 18th Int. Conf. Exhib. Elect. Distrib.*, Turin, Italy, 2005, pp. 1–4.
- [11] I. E. Portugues *et al.*, "RF-based partial discharge early warning system for air-insulated substations," *IEEE Trans. Power Del.*, vol. 24, no. 1, pp. 20–29, Jan. 2009.
- [12] F. Zeng, J. Tang, L. Huang, and W. Wang, "A semi-definite relaxation approach for partial discharge source location in transformers," *IEEE Trans. Dielect. Elect. Insul.*, vol. 22, no. 2, pp. 1097–1103, Apr. 2015.
- [13] E. T. Iorkyase, C. Tachtatzis, P. Lazaridis, I. A. Glover, and R. C. Atkinson, "Radio location of partial discharge sources: A support vector regression approach," *IET Sci., Meas. Technol.*, vol. 12, no. 2, pp. 230–236, Mar. 2017.
- [14] E. T. Iorkyase, C. Tachtatzis, R. C. Atkinson, and I. A. Glover, "Localisation of partial discharge sources using radio fingerprinting technique," in *Proc. Loughborough Antennas Propag. Conf.*, Loughborough, U.K., 2015, pp. 1–5.
- [15] P. J. Moore, I. E. Portugues, and I. A. Glover, "Radiometric location of partial discharge sources on energized high-voltage plant," *IEEE Trans. Power Del.*, vol. 20, no. 3, pp. 2264–2272, Jul. 2005.
- [16] A. R. Mor, P. H. F. Morshuis, P. Llovera, V. Fuster, and A. Quijano, "Localization techniques of partial discharges at cable ends in off-line single-sided partial discharge cable measurements," *IEEE Trans. Dielect. Elect. Insul.*, vol. 23, no. 1, pp. 428–434, Feb. 2016.
- [17] P. J. Moore, I. E. Portugues, and I. A. Glover, "Partial discharge investigation of a power transformer using wireless wideband radio-frequency measurements," *IEEE Trans. Power Del.*, vol. 21, no. 1, pp. 528–530, Jan. 2006.
- [18] L. Qiu and R. A. Kennedy, "Radio location using pattern matching techniques in fixed wireless communication networks," in *Proc. Int. Symp. Commun. Inf. Technol.*, Sydney, Australia, 2007, pp. 1054–1059.
- [19] T. Babnik, R. Aggarwal, and P. Moore, "Data mining on a transformer partial discharge data using the self-organizing map," *IEEE Trans. Dielect. Elect. Insul.*, vol. 14, no. 2, pp. 444–452, Apr. 2007.
- [20] M. S. Abd Rahman, P. L. Lewin, and P. Rapisarda, "Autonomous localization of partial discharge sources within large transformer windings," *IEEE Trans. Dielect. Elect. Insul.*, vol. 23, no. 2, pp. 1088–1098, Apr. 2016.
- [21] J. K. Wong, H. A. Illias, and A. H. A. Bakar, "High noise tolerance feature extraction for partial discharge classification in XLPE cable joints," *IEEE Trans. Dielect. Elect. Insul.*, vol. 24, no. 1, pp. 66–74, Feb. 2017.
- [22] L. Satish and B. Nazneen, "Wavelet-based denoising of partial discharge signals buried in excessive noise and interference," *IEEE Trans. Dielect. Elect. Insul.*, vol. 10, no. 2, pp. 354–367, Apr. 2003.
- [23] D. Evagorou, A. Kyprianou, and P. L. Lewin, "Feature extraction of partial discharge signals using the wavelet packet transform and classification with a probabilistic neural network," *IET Sci., Meas. Technol.*, vol. 4, no. 3, pp. 177–192, May 2010.
- [24] M. Aminghafari, N. Cheze, and J. Poggi, "Multivariate denoising using wavelets and principal component analysis," *Comput. Statist. Data Anal.*, vol. 50, no. 9, pp. 2381–2398, 2006.
- [25] D. A. Jackson, "Stopping rules in principal components analysis: a comparison of heuristical and statistical approaches," *Ecology*, vol. 74, no. 8, pp. 2204–2214, 1993.
- [26] C. Petrarca and G. Lupo, "An improved methodological approach for denoising of partial discharge data by the wavelet transform," *Prog. Electromagn. Res.*, vol. 58, pp. 205–217, 2014.
- [27] B. T. Phung, Z. Liu, T. R. Blackburn, and R. E. James, "Wavelet transform analysis of partial discharge signals," in *Proc. Australasian Uni. Power Eng. Conf.*, Darwin, Australia, 1999, pp. 1–7.
- [28] U. Khayam and T. Kasnalestari, "System of wavelet transform on partial discharge signal denoising," in *Proc. Int. Conf. Ind., Mech., Elect., Chem. Eng.*, Yogyakarta, Indonesia, 2016, pp. 79–83.
- [29] E. C. T. Macedo *et al.*, "Wavelet transform processing applied to partial discharge evaluation," *J. Phys.: Conf. Ser.*, vol. 364, no. 1, pp. 12–54, 2012.
- [30] Q. Shan *et al.*, "Characteristics of impulsive noise in electricity substations," in *Proc. 17th Eur. Signal Process. Conf.*, 2009, pp. 2136–2140.
- [31] M. Homaei, S. M. Moosavian, and H. A. Illias, "Partial discharge localization in power transformers using neuro-fuzzy technique," *IEEE Trans. Power Del.*, vol. 29, no. 5, pp. 2066–2076, Oct. 2014.
- [32] T. Li and M. Zhou, "ECG classification using wavelet packet entropy and random forests," *Entropy*, vol. 18, no. 8, pp. 285–300, 2016.
- [33] C. S. Chang, J. Jin, C. Chang, T. Hoshino, M. Hanai, and N. Kobayashi, "Separation of corona using wavelet packet transform and neural network for detection of partial discharge in gas-insulated substations," *IEEE Trans. Power Del.*, vol. 20, no. 2, pp. 1363–1369, Apr. 2005.
- [34] S. Anjum, S. Jayaram, A. El-Hag, and A. N. Jahromi, "Detection and classification of defects in ceramic insulators using RF antenna," *IEEE Trans. Dielect. Elect. Insul.*, vol. 24, no. 1, pp. 183–190, Feb. 2017.
- [35] Z. Ye, B. Wu, and A. Sadeghian, "Current signature analysis of induction motor mechanical faults by wavelet packet decomposition," *IEEE Trans. Ind. Electron.*, vol. 50, no. 6, pp. 1217–1228, Dec. 2003.
- [36] M. M. Eissa, "A novel digital directional transformer protection technique based on wavelet packet," *IEEE Trans. Power Del.*, vol. 20, no. 3, pp. 1830–1836, Jul. 2005.
- [37] J. Li, T. Jiang, R. F. Harrison, and S. Grzybowski, "Recognition of ultra high frequency partial discharge signals using multi-scale features," *IEEE Trans. Dielect. Elect. Insul.*, vol. 19, no. 4, pp. 1412–1420, Aug. 2012.
- [38] M. Varanis and R. Pederiva, "The influence of the wavelet filter in the parameters extraction for signal classification: An experimental study," in *Proc. Ser. Brazilian Soc. Comput. Appl. Maths.*, vol. 5, no. 1, 2017, pp. 10501-1–10501-7.
- [39] A. Swetapadma and A. Yadav, "A novel decision tree regression-based fault distance estimation scheme for transmission lines," *IEEE Trans. Power Del.*, vol. 32, no. 1, pp. 234–245, Feb. 2017.
- [40] D. Sanchez-Rodriguez, P. Hernandez-Morera, J. Quinteiro, and I. Alonso-Gonzalez, "A low complexity system based on multiple weighted decision trees for indoor localization," *Sensors*, vol. 15, no. 6, pp. 14809–14829, 2015.
- [41] H. Ahmadi and R. Bouallegue, "RSSI-based localization in wireless sensor networks using Regression Tree," in *Proc. Int. Wireless Commun. Mobile Comput. Conf.*, Dubrovnik, Croatia, 2015, pp. 1548–1553.
- [42] M. M. bin Othman, A. Mohamed, and A. Hussain, "Determination of transmission reliability margin using parametric bootstrap technique," *IEEE Trans. Power Syst.*, vol. 23, no. 4, pp. 1689–1700, Nov. 2008.
- [43] D. Den Hertog, J. P. C. Kleijnen, and A. Y. D. Siem, "The correct Kriging variance estimated by bootstrapping," *J. Oper. Res. Soc.*, vol. 57, no. 4, pp. 400–409, 2006.
- [44] A. K. Jain, R. C. Dubes, and C. Chen, "Bootstrap techniques for error estimation," *IEEE Trans. Pattern Anal. Mach. Intell.*, vol. PAMI-9, no. 5, pp. 628–633, Sep. 1987.
- [45] A. Criminisi *et al.*, "Regression forests for efficient anatomy detection and localization in computed tomography scans," *Med. Image Anal.*, vol. 17, no. 8, pp. 1293–1303, 2013.
- [46] X. Xie, J. Xing, N. Kong, C. Li, J. Li, and S. Zhang, "Improving colorectal polyp classification based on physical examination data—an ensemble learning approach," *IEEE Robot. Autom. Lett.*, vol. 3, no. 1, pp. 434–441, Jan. 2018.
- [47] A. Kacete, J. Royan, R. Seguier, M. Collobert, and C. Soladie, "Real-time eye pupil localization using Hough regression forest," in *Proc. IEEE Winter Conf. Appl. Comput. Vis.*, Lake Placid, NY, USA, 2016, pp. 1–8.
- [48] H. Mohamed *et al.*, "Partial discharge localization based on received signal strength," in *Proc. 23rd Int. Conf. Autom. Comput.*, Huddersfield, U.K., 2017, pp. 1–4.
- [49] U. F. Khan *et al.*, "An efficient algorithm for partial discharge localization in high-voltage systems using received signal strength," *Sensor*, vol. 18, no. 11, 2018, Art. no. 4000.
- [50] Z. Li, L. Luo, Y. Liu, G. Sheng, and X. Jiang, "UHF partial discharge localization algorithm based on compressed sensing," *IEEE Trans. Dielect. Elect. Insul.*, vol. 25, no. 1, pp. 21–29, Feb. 2018.
- [51] M. Zhu *et al.*, "Localization of multiple partial discharge sources in air-insulated substation using probability-based algorithm," *IEEE Trans. Dielect. Elect. Insul.*, vol. 24, no. 1, pp. 157–166, Feb. 2017.
- [52] D. K. Mishra, B. Sarkar, C. Koley, and N. K. Roy, "An unsupervised Gaussian mixer model for detection and localization of partial discharge sources using RF sensors," *IEEE Trans. Dielect. Elect. Insul.*, vol. 24, no. 4, pp. 2589–2598, Jan. 2017.
- [53] Z. Li, L. Luo, N. Zhou, G. Sheng, and X. Jiang, "A novel partial discharge localization method in substation based on a wireless UHF sensor array," *Sensors*, vol. 17, no. 8, 2017, Art. no. 1909.